atoms

IMPACT FACTOR 1.5

CITESCORE 3.1

Article

Multi-Configuration Dirac–Hartree–Fock Calculations of Pr^{9+} and Nd^{10+}: Configuration Resolution and Probing Fine-Structure Constant Variation

Songya Zhang, Cunqiang Wu, Chenzhong Dong and Xiaobin Ding

Special Issue

Atomic and Molecular Data and Their Applications: ICAMDATA 2024

Edited by

Prof. Dr. Chenzhong Dong, Prof. Dr. Xiaobin Ding, Prof. Dr. Denghong Zhang, Prof. Dr. Maogen Su and Prof. Dr. Jun Jiang

MDPI

https://doi.org/10.3390/atoms13060054

atoms

MDPI

Article

Multi-Configuration Dirac–Hartree–Fock Calculations of Pr^{9+} and Nd^{10+}: Configuration Resolution and Probing Fine-Structure Constant Variation

Songya Zhang [1], Cunqiang Wu [1,2], Chenzhong Dong [1,2] and Xiaobin Ding [1,2,3,*]

[1] Key Laboratory of Atomic and Molecular Physics and Functional Materials of Gansu Province, College of Physics and Electronic Engineering, Northwest Normal University, Lanzhou 730070, China; dongcz@nwnu.edu.cn (C.D.)
[2] Gansu International Scientific and Technological Cooperation Base of Laser Plasma Spectroscopy, Lanzhou 730070, China
[3] Gansu Provincial Research Center for Basic Discipline of Quantum Physics, Lanzhou 730070, China
* Correspondence: dingxb@nwnu.edu.cn

Abstract: We present high-precision multi-configuration Dirac–Hartree–Fock (MCDHF) calculations for the metastable states of Pr^{9+} and Nd^{10+} ions, systematically investigating their energy levels, transition properties, Landé g_J factors, and hyperfine interaction constants. Our results show excellent agreement with available experimental data and theoretical benchmarks, while resolving critical configuration assignment discrepancies through detailed angular momentum coupling analysis. The calculations highlight the significant role of Breit interaction and provide the first theoretical predictions of electric quadrupole hyperfine constants (B_{hfs}). These findings deliver essential atomic data for the development of next-generation optical clocks and establish lanthanide highly charged ions as exceptional candidates for precision tests of fundamental physics.

Keywords: energy levels; landé g factor; hyperfine interaction constants; breit interaction; multi-configuration dirac–hartree–fock

Academic Editor: Yew Kam Ho

Received: 11 May 2025
Revised: 9 June 2025
Accepted: 11 June 2025
Published: 16 June 2025

Citation: Zhang, S.; Wu, C.; Dong, C.; Ding, X. Multi-Configuration Dirac–Hartree–Fock Calculations of Pr^{9+} and Nd^{10+}: Configuration Resolution and Probing Fine-Structure Constant Variation. *Atoms* **2025**, *13*, 54. https://doi.org/10.3390/atoms13060054

1. Introduction

Highly Charged Ions (HCIs) are not only ubiquitously present in astrophysical environments but also extensively observed in several experimental systems, including magnetic confinement fusion devices, electron beam ion traps (EBITs), heavy-ion accelerators, and laser-produced plasmas [1–4]. Forbidden transitions in HCIs have long been a central focus in both astrophysical spectroscopy and laboratory plasma physics due to their high diagnostic potential [5,6]. The spectral line intensities of transitions from HCIs exhibit extreme sensitivity to plasma density and temperature, making them critical tools for diagnosing and modeling both astrophysical environments and laboratory plasmas [7–9]. Moreover, forbidden transitions in HCIs are promising candidates for next-generation optical atomic clocks and for probing potential temporal variations of fundamental constants [10–12]. Recent advances in many-body theoretical frameworks have also highlighted their suitability for precision tests of quantum electrodynamics (QED) in strong-field regimes [13–15].

Owing to their contracted electron clouds and enhanced relativistic effects, HCIs exhibit exceptional insensitivity to external perturbations while maintaining pronounced sensitivity to variations in the fine-structure constant α. These properties render them highly suitable for the development of ultra-stable optical clocks [16–19]. However, only a limited number of HCIs systems have demonstrated viable optical-clock transitions.

A representative mechanism involves magnetic dipole ($M1$) or electric quadrupole ($E2$) transitions between fine or hyperfine structures levels. In isoelectronic sequences of HCIs, the increasing nuclear charge Z systematically enlarges energy gaps between fine-structure levels and enhances hyperfine splitting. This progression shifts transition frequencies from the microwave to the optical frequency regimes [20,21]. Notably, the rearrangements of orbital binding energies within these sequences can induce energy level crossings. At these critical points, near-degenerate levels produce dense optical transitions with laser-accessible frequencies in the visible spectrum [22,23]. Together, these characteristics establish HCIs as promising platforms for precision spectroscopy and next-generation optical frequency standards [24–27].

Energy level crossings in HCIs have long been of interest in atomic structure studies [28–30]. Systematic analyses have identified multiple HCIs with potential for optical clock applications, including the low-lying excited states in open shells configurations of ions such as Nd^{n+} ($n = 4, 5$) [29], Ba^{4+} [31], Pr^{9+} [32], Cf^{6+} and Cf^{7+} [33], and Nd^{9+} [34]. As the charge state increases, the evolution of electronic structure in HCIs leads to a fundamental change in orbital ordering: electron filling rules gradually transition from Madelung's rule to hydrogen-like (Coulomb) limit. This structural rearrangement results in characteristic level crossings, particularly involving s–d, s–f, and p–f orbitals. Many studies have focused on these phenomenon in ions such as Nd^{13+}, Cf^{15+} and Sm^{14+} [35,36], Ir^{17+}, Ir^{16+}, W^{7+}, and W^{8+} [37], in efforts to assess their suitability for optical frequency metrology.

Experimentally, optical clocks based on neutral atoms Sr and singly charged ions, such as Al^{+} and Yb^{+}, have already achieved fractional frequency uncertainties at the 10^{-18}–10^{-19} levels [19,25,38]. Theoretical studies suggest that HCI-based optical clocks could surpass these systems, potentially achieving accuracies on the order of 10^{-20}–10^{-21} [39–41]. Recently, clock transitions in Ar^{13+} have been successfully demonstrated using quantum logic spectroscopy [42]. In the Sn-like isoelectronic sequence, Pr^{9+} and Nd^{10+} ions have emerged as particularly promising candidates due to relativistic $5p$–$4f$ orbital crossings (see Figure 1). Among these, Pr^{9+} is especially attractive due to its unique electronic configuration [32,43]. The $5p^2\ ^3P_0 \rightarrow 5p4f\ ^3G_3$ magnetic octupole ($M3$) transition in Pr^{9+} is an excellent candidate for ultra-precise optical clocks and searches for physics beyond the Standard Model, as it exhibiting high sensitivity to both fine-structure constant α variations and potential violations of local Lorentz invariance (LLI) [44,45]. Additionally, the strong $M1$ transition at 351 nm ($5p^2\ ^3P_0 \rightarrow ^3P_1$) provides a feasible path for ion cooling and probing.

Current research efforts are directed toward identifying narrow-linewidth clock transitions in HCIs such as Ni^{12+}, Pd^{12+}, Pr^{9+}, and Nd^{9+} [32,34,46,47]. However, current theoretical predictions still lack the accuracy required to guide the precision laser spectroscopy experiments.

In this work, we employ the multi-configuration Dirac–Hartree–Fock (MCDHF) method to systematically investigate key atomic parameters of the highly charged ions Pr^{9+} and Nd^{10+}, including energy levels, transition wavelengths, transition probabilities, Landé g factors, and hyperfine interaction constants. Our calculated results show excellent agreement with both existing theoretical data and recent experimental measurements. These results are expected to provide valuable reference data for the development of high-precision optical clocks and for plasma diagnostics in astrophysics contexts.

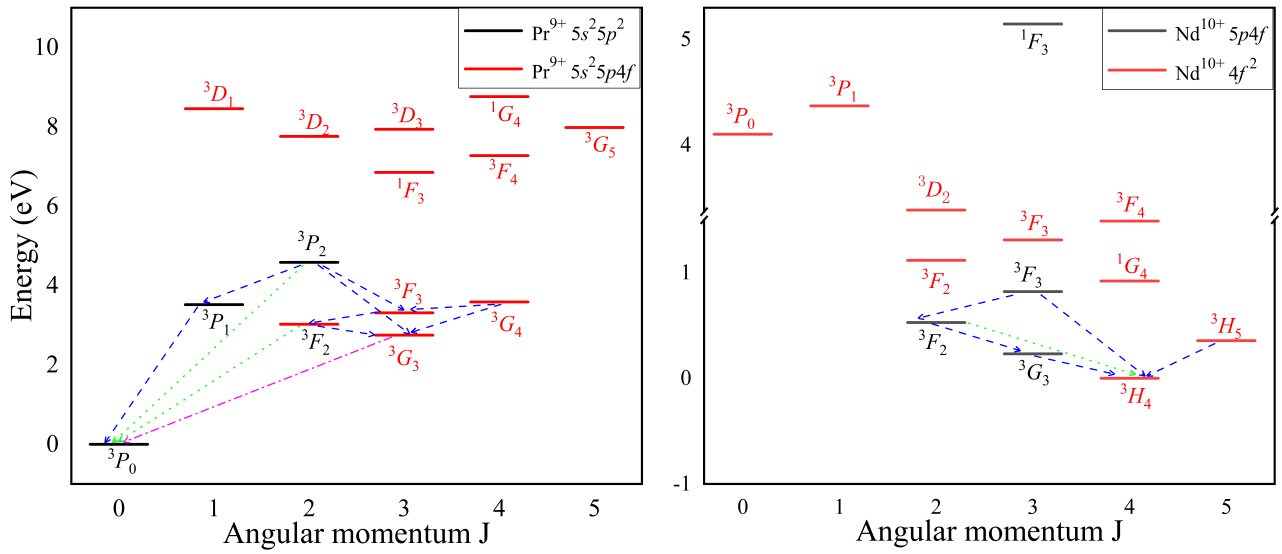

Figure 1. The energy level structure diagram of Pr^{9+} and Nd^{10+} ions. The blue dashed arrow represents *M*1 transition, the green dotted arrow represents *E*2 transition, and magenta dash-dot arrow represents *M*3 transition.

2. Results and Discussion

Utilizing the MCDHF method with the aforementioned electron correlation model, we systematically calculated excitation energies, transition energies, transition probabilities, lifetimes, Landé g factors, hyperfine interaction constants, and the sensitivity coefficients to the variation in the fine-structure constant α for Pr^{9+} and Nd^{10+} ions.

2.1. Energy Levels of Pr^{9+} and Nd^{10+} Ions

Table 1 presents the excitation energies for selected energy levels arising from the $5p^2$, $5p4f$, and $4f^2$ configurations of Pr^{9+} and Nd^{10+} ions. All the levels are denoted by LS notation obtained by the *jj2lsj* code from the GRASP2k package. This computation enables us to estimate the dominant LS-coupling character inherent to each state. The LS term labels, in turn, are assigned according to the largest component present in the configuration state function (CSF) expansion. The numbers in the parentheses indicate the estimated uncertainty of the available data. The accuracy of our calculation was assessed using an extrapolation approach similar to that described by Fischer [48]. Specifically, we evaluated the convergence behavior of the excitation energy by firstly computing difference between successive active space expansion: $\Delta E_{AS6} = E_{AS6} - E_{AS5}$ and $\Delta E_{AS5} = E_{AS5} - E_{AS4}$. Then, the rate of convergence is estimated as

$$r = \Delta E_{AS6}/\Delta E_{AS5}.$$

Assuming that this convergence rate remains constant in the subsequent steps, the residual contribution can be approximated by a geometric series, yielding a total correction of

$$\sum_{i=1}^{\infty} \Delta E_{AS6} r^i = \Delta E_{AS6} \frac{r}{1-r} \quad \text{if } |r| < 1.$$

It should be noted, however, that this approach may underestimate the remaining corrections, as contributions from higher active spaces often converge slowly, potentially leading to an increasing ratio r at larger configuration expansions.

Table 1. Contributions of the Breit interaction and QED effects to the excitation energy (in cm^{-1}) of selected levels in Pr^{9+} and Nd^{10+}. Bold font indicates levels with ambiguous term assignments. Diff = |Final − Expt|/Final × 100%. The digits in the parentheses indicates the accuracy of the available data.

Ion	Ref [32]	Config (Term)	Coulomb	Breit	QED	Final	AMBiT [32]	FSCC [32]	CI + all Order [43]	Expt [32]	Diff (%)
Pr^{9+}	$5p^2\ [^3P_0]$	$5p^2\ [^3P_0]$	0	0	0	0	0	0	0	0	0
	$5p4f\ [^3G_3]$	$5p4f\ [^3G_3]$	22,848	−642	−11	22,195 (4)	21,368	22,248	21,055 (840)	22,101.36 (5)	0.42
	$5p4f\ [^3F_2]$	$5p4f\ [^3F_2]$	24,993	−607	−4	24,382 (3)	23,845	24,525	23,845 (710)	24,494.00 (5)	0.46
	$5p4f\ [^3\mathbf{D}_3]$	$5p4f\ [^3\mathbf{F}_3]$	27,644	−917	−8	26,720 (3)	26,372	27,575	26,182 (820)	27,287.09 (5)	2.12
	$5p^2\ [^3P_1]$	$5p^2\ [^3P_1]$	28,753	−412	45	28,386 (2)	27,789	28,526	28,440 (900)	28,561.06 (6)	0.62
	$5p4f\ [^3G_4]$	$5p4f\ [^3G_4]$	29,897	−949	−8	28,940 (3)	28,369	29,482	28,474 (320)	29,230.87 (6)	1.01
	$5p^2\ [^3\mathbf{D}_2]$	$5p^2\ [^3\mathbf{P}_2]$	37,467	−513	42	36,997 (1)	35,550	35,980	35,935 (380)	36,407.48 (6)	1.59
	$5p4f\ [^3\mathbf{F}_3]$	$5p4f\ [^1\mathbf{F}_3]$	56,305	−1072	36	55,269 (9)	54,852	55,737	54,404 (820)	55,662.43 (5)	0.71
	$5p4f\ [^3F_4]$	$5p4f\ [^3F_4]$	59,898	−1254	37	58,681 (10)	58,469	59,393		59,184.84 (5)	0.86
	$5p^2\ [^3\mathbf{F}_2]$	$5p4f\ [^3\mathbf{D}_2]$	63,547	−1005	45	62,587 (17)	61,325	62,380		62,182.14 (2)	0.65
	$5p4f\ [^3G_5]$	$5p4f\ [^3G_5]$	65,312	−1317	36	64,031 (11)	62,788	64,214		63,924.17 (6)	0.17
	$5p4f\ [^3D_1]$	$5p4f\ [^3D_1]$	69,229	−1048	66	68,217 (10)	66,429	67,925		67,309.3 (1)	1.36
Nd^{10+}		$4f^2\ [^3H_4]$	0	0	0	0			0		
		$5p4f\ [^3G_3]$	978	881	13	1872 (1)			1062 (1300)		
		$4f^2\ [^3H_5]$	3185	−310	2	2877 (1)			3059 (210)		
		$5p4f\ [^3F_2]$	3535	718	13	4265 (2)			4550 (1100)		
		$5p4f\ [^3F_3]$	6180	427	15	6621 (1)			6738 (1320)		
		$4f^2\ [^1G_4]$	7276	153	10	7437 (2)					

For Pr^{9+}, our results show excellent agreement with recent experimental values and previous theoretical predictions, with deviations generally within 2% after accounting for Breit interaction and QED effects. This accuracy indicates that dominant correlation and relativistic effects are well captured by the adopted calculation model.

Several term assignments exhibit discrepancies between experimental observation and theoretical calculation, echoing findings from S. G. Porsev et al. [49]. Specifically, the level experimentally labeled as $5p4f\ ^3D_3$ is theoretically identified as $[^3F_3]$; the $5p^2\ ^3D_2$ term corresponds to the $^3P_2$ term; and the $^3F_2$ level arises not from the $5p^2$ configuration but from $5p4f$. This is consistent with atomic structure theory, as two equivalent p electrons cannot generate a term with total orbital angular momentum $L = 3$. Additionally, the state associated with the $5p4f$ configuration is more appropriately designated as $^1F_3$, not $^3F_3$.

Breit interaction corrections contribute up to 3% of the excitation energies in Pr^{9+}, while QED contributions are negligible. Our results also exhibit strong consistency with other theoretical models, such as AMBiT and FSCC, further validating the reliability of our MCDHF approach. In Nd^{10+}, the Breit interaction exhibits an even more pronounced influence, reaching up to 47% for some states. Although the CI+all-order calculations present relatively large uncertainties, our results fall within their estimated ranges, thereby offering valuable benchmark. These systematic data are particularly important for advancing high-precision optical clocks development and provide a foundation for future experimental studies, especially for Nd^{10+}, where experimental data remain limited.

2.2. Transition Properties

Table 2 lists transition properties, including transition energies, types, probabilities, and lifetimes for key transitions in Pr^{9+} and Nd^{10+}. The computed values show excellent agreement with experimental transition energies, typically within 0.1–0.2 eV. Transition probabilities calculated using the MCDHF method also align well with those from CI+all-order methods [43].

For Pr^{9+}, the M3 transition from the $5p4f\ [^3G_3]$ level to the ground state ($5p^2\ [^3P_0]$) has a very small rate ($\sim 10^{-15}$ s^{-1}), resulting in a long lifetime on the order of 10^{14} s. Conversely, the E2 transition from $5p4f\ [^3F_2]$ to $5p^2\ [^3P_0]$ has a rate on the order of 10^{-2} s^{-1}, giving a lifetime in the tens of seconds range. Several M1 transitions among closely spaced levels also exhibit significant transition probabilities, contributing to observable decay channels.

The consistency of transition rates across methods and with available experimental data supports the reliability of our electron correlation model. These accurate predictions of lifetimes and branching ratios are critical for identifying suitable clock transitions and for interpreting astrophysical spectra.

Table 2. Comparison of the transition energies ΔE (eV) and transition probabilities(s^{-1}) for selected transitions in Pr^{9+} and Nd^{10+}. Asterisks denote direct experimental observations.

				ΔE						Rate		τ	
Ion	**Upper**	**Lower**	**Type**	**MCDHF**	**Expt [32]**	**AMBiT [32]**	**FSCC [32]**	**CI + all Order [43]**	**λ (nm)**	**MCDHF**	**Ref. [43]**	**MCDHF**	**Ref. [43]**
Pr^{9+}	$5p4f[^3G_3]$	$5p^2[^3P_0]$	M3	2.75	2.74	2.65	2.76	2.71	451	4.32 [−15]	2.00 [−15]	2.32 [+14]	4.99 [+14]
	$5p4f[^3F_2]$	$5p^2[^3P_0]$	E2	3.02	3.04	2.96	3.04	3.00	410	3.43 [−02]	8.64 [−01]	2.3 [+01]	5.18 [+01]
	$5p4f[^3F_2]$	$5p4f[^3G_3]$	M1	0.27	0.30	0.31	0.28	0.29	4573	9.12 [−03]	7.92 [−03]		
	$5p4f[^3F_3]$	$5p4f[^3F_2]$	M1	0.29	0.35	0.31	0.38	0.35	4278	1.54 [−01]	2.12 [−01]	6.49 [+00]	4.72 [+00]
	$5p^2[^3P_1]$	$5p^2[^3P_0]$	M1	3.52	3.54 *	3.45	3.54	3.53	352	3.38 [+02]	3.36 [+02]	2.94 [−03]	2.98 [−03]
	$5p4f[^3G_4]$	$5p4f[^3G_3]$	M1	0.84	0.88	0.87	0.90	0.92	1483	3.34 [+00]	4.32 [+00]	2.93 [−01]	2.27 [−01]
	$5p4f[^3G_4]$	$5p4f[^3F_3]$	M1	0.28	0.24	0.25	0.24	0.29	1483	7.04 [−02]	7.39 [−02]		
	$5p^2[^3P_2]$	$5p^2[^3P_0]$	E2	4.59	4.51	4.41	4.46	4.49	270	4.91 [+00]	4.85 [+00]	7.70 [−02]	8.38 [−02]
	$5p^2[^3P_2]$	$5p4f[^3G_3]$	M1	1.84	1.77	1.76	1.70	1.78	675	7.28 [−01]	7.46 [−01]		
	$5p^2[^3P_2]$	$5p4f[^3F_3]$	M1	1.27	1.13	1.14	1.04	1.14	973	3.40 [+00]	4.16 [+00]		
	$5p^2[^3P_2]$	$5p^2[^3P_1]$	M1	1.07	1.22	0.96	0.92	0.96	1161	3.91 [+00]	2.20 [+00]		
	$5p4f[^3D_2]$	$5p^2[^3P_2]$	M3	3.26	3.20 *	3.20	3.27		380	9.63 [−14]		1.14 [−02]	
	$5p4f[^3D_2]$	$5p^2[^3P_1]$	M1	4.21	4.17 *	4.16	4.20		295	8.75 [+01]			
Nd^{10+}	$5p4f[^3G_3]$	$4f^2[^3H_4]$	M1	0.23				0.19	5347	1.41 [−04]	1.96 [−05]	7.10 [+03]	5.09 [+04]
	$4f^2[^3H_5]$	$4f^2[^3H_4]$	M1	0.36				0.38	3475	6.09 [−01]	7.26 [−01]	1.64 [+00]	1.38 [+00]
	$5p4f[^3F_2]$	$5p4f[^3G_3]$	M1	0.30				0.30	4171	2.08 [−02]	3.95 [−02]	4.81 [+01]	2.54 [+01]
	$5p4f[^3F_2]$	$4f^2[^3H_4]$	E2	0.53				0.63	2345	1.13 [−05]	1.94 [−05]		
	$5p4f[^3F_3]$	$5p4f[^3F_2]$	M1	0.29				0.25	4243	2.02 [−01]	1.53 [−01]	4.79 [+00]	3.92 [+00]
	$5p4f[^3F_3]$	$4f^2[^3H_4]$	M1	0.82				0.87	1510	6.72 [−03]	5.97 [−03]		

2.3. Hyperfine Interaction Constant and Landé g Factor

The hyperfine interaction arises from the interaction between the magnetic moments of the electrons and the magnetic moments of the nucleus in an atom. In the first-order approximation, the energy splitting due to the hyperfine interaction is given by

$$\Delta E_{\mathrm{hfs}} = \frac{1}{2} A_{\mathrm{hfs}} C + B_{\mathrm{hfs}} \frac{\frac{3}{4}C(C+1) - I(I+1)J(J+1)}{2I(2I-1)J(2J-1)} \tag{1}$$

where $C = F(F+1) - J(J+1) - I(I+1)$, I and J represent the nuclear and atomic angular momenta, respectively. F is the total angular momenta quantum numbers coupling by I and J. A_{hfs} and B_{hfs} are known as the magnetic dipole and electric quadrupole hyperfine interaction constants. With the knowledge of A_{hfs} and B_{hfs}, it is possible to estimate ΔE for any hyperfine level F. For the ions considered in this work ($^{141}_{59}\mathrm{Pr}^{9+}$ with I = 5/2 and $^{145}_{60}\mathrm{Nd}^{10+}$ with I = −7/2), we have calculated the magnetic dipole and electric quadrupole constants corresponding to different nuclear spins respectively. The magnetic dipole constants can be calculated using the following expression:

$$A_{\mathrm{hfs}} = \frac{\mu_I}{I} \sqrt{\frac{1}{J(J+1)}} \langle \Psi(\gamma J) \| \boldsymbol{T}^{(1)} \| \Psi(\gamma J) \rangle \tag{2}$$

$$B_{\mathrm{hfs}} = 2Q_I \sqrt{\frac{J(2J-1)}{(J+1)(2J+3)}} \left\langle \Psi(\gamma J) \| \boldsymbol{T}^{(2)} \| \Psi(\gamma J) \right\rangle \tag{3}$$

where μ_I and Q_I are the magnetic dipole moment and the quadrupole moment of the nucleus, respectively. The values of the magnetic dipole moment and electronic quadrupole moment of $^{141}_{59}\mathrm{Pr}^{9+}$($\mu_I$ = 4.2754μ_N, Q = −0.0776b), and $^{145}_{60}\mathrm{Nd}^{10+}$ (μ_I = −1.065μ_N, Q = −0.593b), were taken from the work of Stone et al. [50].

The Landé g-factor reflects the sensitivity of the atomic state to the external magnetic field and plays a key role in diagnosing the magnetic field strength [51–53]. Within the framework of relativistic atomic structure theory, the Landé g_J factor can be calculated using the reduced matrix element of $M1$. The Landé g_J factor is given by [54–56]:

$$g_J = -\frac{1}{2\mu_B} \frac{\langle \Psi(\gamma J) \| Q^{M1} \| \Psi(\gamma J) \rangle}{\sqrt{J(J+1)(2J+1)}} \tag{4}$$

where μ_B denotes the Bohr magneton. Once the Landé g_J-factor for a specific atomic state is determined, the energy of the split levels can be accurately calculated. This allows for the determination of the first order Zeeman shift [57,58], given by

$$\Delta E^{(1)}_{\mathrm{Zeem}} = g_J \mu_B M B \tag{5}$$

where B is the magnetic flux density of the external field, and M is the magnetic quantum number.

Table 3 presents calculated hyperfine magnetic dipole (A) and electric quadruple (B) constants, and Landé g_J-factor for low-lying states of Pr^{9+} and Nd^{10+}. The values are computed using nuclear parameters appropriate for the most abundant isotopes, ^{141}Pr and ^{143}Nd. These data are essential for interpreting hyperfine splitting in high-resolution spectra and for precision frequency metrology.

Table 3. Hyperfine magnetic dipole (A) and electric quadrupole (B) constants, and the Landé g_J-factor of low-lying levels in Pr^{9+} and Nd^{10+} ions. The nuclear spin $I = 5/2$ and magnetic moment $\mu = 4.2754\ (5)\ \mu_N$ were used for Pr^{9+}, and $I = 7/2$, $\mu = -1.5290\ (2)\ \mu_N$ for Nd^{10+}.

			Hyperfine Constant (GHz)			Landé g_J-Factor		
Ion	**Config**	**Level**	$A_{\mathbf{hfs}}$	**AMBiT** [32]	$B_{\mathbf{hfs}}$	**MCDHF**	**AMBiT** [32]	**Expt** [32]
Pr^{9+}	$5p^2$	$^3P_0$	0	0	0	0	0	0
	$5p4f$	$^3G_3$	7.631	7.771	0.075	0.857	0.853	0.875 (2)
	$5p4f$	$^3F_2$	−2.434	−1.688	0.012	0.841	0.883	0.889 (5)
	$5p4f$	$^3F_3$	−3.572	−3.857	0.119	1.138	1.145	1.136 (4)
	$5p^2$	$^3P_1$	−2.967	−3.203	−0.256	1.500	1.500	1.487 (3)
	$5p4f$	$^3G_4$	5.343	5.692	0.190	1.122	1.115	1.130 (3)
	$5p^2$	$^3P_2$	11.467	11.004	−0.104	1.187	1.139	1.19 (1)
Nd^{10+}	$4f^2$	$^3H_4$	0.281		−0.057	0.806		
	$5p4f$	$^3G_3$	1.637		0.063	0.854		
	$4f^2$	$^3H_5$	0.214		0.034	1.032		
	$5p4f$	$^3F_2$	−0.645		0.069	0.774		
	$5p4f$	$^3F_3$	−0.612		0.083	1.136		
	$4f^2$	$^1G_4$	0.680		−0.078	1.109		

Hyperfine magnetic dipole constants (A) show considerable variation among different states, depending strongly on the electronic configuration and the angular momentum coupling of the electrons near the nucleus. For Pr^{9+}, the A constants range from a few GHz to over 11 GHz. The large values for some $5p4f$ states arise due to significant overlap of the $4f$ orbital with the nucleus, enhancing hyperfine interactions. Similarly, quadrupole constants (B) are sizeable for states with $J \geq 1$ and reflect the distribution of electronic charge around the nucleus.

These hyperfine constants are of particular importance for experimental efforts in high-resolution laser spectroscopy. They allow accurate modeling of hyperfine splittings which are crucial for determining systematic frequency shifts in atomic clocks based on highly charged ions. Furthermore, they offer a benchmark for refining nuclear models and probing nuclear moments through atomic spectroscopy.

The Landé g-factors for all levels are in good agreement with both the theoretical results from AMBiT and the experimental results [32]. Nevertheless, for the Nd^{10+} ion, there are no comparable results at present. We hope that these calculated results can provide a reference for future experimental studies or theoretical analyses.

2.4. Sensitivity of Clock Transitions

The frequencies of optical atomic clock transitions exhibit different dependencies on the fine-structure constant, enabling high-precision tests of its possible variation over time or space [45,59]. By monitoring the ratio of two clock transition frequencies over an extended period, any observed change in this ratio may signal a variation in α. Crucially, this ratio is dimensionless and independent of the system of units used.

In atomic units, the relativistic correction to atomic energy levels scale approximately as α^2, which leads to a convenient parameterization of the transition frequency ω as

$$\omega = \omega_0 + q\left[\left(\frac{\alpha}{\alpha_0}\right)^2 - 1\right] \tag{6}$$

where ω_0 is the unperturbed transition frequency at the reference value α_0 of the fine structure constant, and q is the sensitivity coefficient. The coefficient q quantifies how strongly the transition frequency shifts with small changes in α and can be accurately determined

through atomic structure calculations. Notably, q is less sensitive to electron correlation effects than absolute energy levels, making it more robust for precision evaluation.

To compute the q coefficient, one performs atomic structure calculations with two slightly different values of α^2, introducing a small, controlled perturbations[60,61]. The coefficient is then extracted via numerical differentiation as follows:

$$q = \frac{\omega(x) - \omega(-x)}{2x} \tag{7}$$

where $x = (\alpha/\alpha_0)^2 - 1$. The perturbation parameter x must be small enough to ensure linear behavior, yet large enough to suppress numerical noise; in our calculation, we take $x = 0.01$.

To detect a possible change in α, one must compare at least two independent clock transitions over time. The fractional variation in their frequency ratio can be expressed as

$$\delta\left(\frac{\omega_1}{\omega_2}\right) / \frac{\omega_1}{\omega_2} = \frac{\delta\omega_1}{\omega_1} - \frac{\delta\omega_2}{\omega_2} \equiv (K_1 - K_2)\frac{\delta\alpha}{\alpha} \tag{8}$$

where $K = 2q/\omega$ is the dimensionless enhancement factor. A larger K value indicates high sensitivity of a transition frequency to changes in α, making such transitions ideal for probing its variation.

Table 4 presents the computed q values and enhancement factors K for several low-lying levels in Pr^{9+} and Nd^{10+}. All the listed transitions exhibit enhancement factors significantly larger than unity, confirming their exceptional sensitivity to α-variation. Particularly striking are the levels in Nd^{10+}, where K values reach as high as -84.6, surpassing those found in many currently operational optical clocks, including those based on neutral atoms, singly charged ions, and some HCIs.

Table 4. Sensitivity coefficients (q) and enhancement factor (K) for selected transitions in Pr^{9+} and Nd^{10+} ions.

Ion	Config	Level	ω (cm^{-1})	q	K
Pr^{9+}	$5p4f$	$^3G_3$	22,184.96	46,027	4.1
	$5p4f$	$^3F_2$	24,376.09	46,020	3.8
	$5p4f$	$^3F_3$	26,710.83	51,206	3.8
	$5p^2$	$^3P_1$	28,380.26	36,608	2.6
	$5p4f$	$^3G_4$	28,931.23	51,206	3.5
	$5p^2$	$3P_2$	36,995.13	42,944	2.3
Nd^{10+}	$5p4f$	$^3G_3$	1871.53	−79,197	−84.6
	$5p4f$	$^3F_2$	4265.37	−60,108	−28.2
	$5p4f$	$^3F_3$	6621.39	−76,526	−23.1
	$4f^2$	$^1G_4$	7437.39	−43,269	−11.6
	$4f^2$	$^3F_2$	9011.82	−27,591	−6.1

The heightened sensitivity arises from strong relativistic effects associated with $5p - 4f$ orbital interactions. The relativistic contraction of $5p$ orbitals, combined with the relatively unperturbed nature of $4f$ orbitals, leads to a pronounced dependence of the transition energy on α. This $5p - 4f$ hybridization mechanism makes these lanthanide HCIs particularly powerful for fundamental physics searches, including tests of temporal variation of fundamental constants and violations of local Lorentz invariance.

3. Theory and Methods

3.1. Multi-Configuration Dirac–Hartree–Fock Method

To accurately predict the transition energies and lifetimes of clock states, we employ the *ab initio* fully relativistic Multi-Configuration Dirac–Hartree–Fock (MCDHF) method, followed by the Relativistic Configuration Interaction (RCI) approach. These methods are implemented in the GRASP2K code package [62–64]. For detailed methodological background, readers are referred to Froese Fischer [65] and the monograph by I. P. Grant [66]. This framework has been successfully applied in recent studies of complex atomic structures and related properties [67,68].

In the MCDHF method, an atomic state wave function is represented by a linear combination of configuration state functions (CSFs) Φ with common parity P, total angular momentum J, and its component M_J:

$$\Psi(\gamma PJM_J) = \sum_{i=1}^{N_c} c_i \Phi(\gamma_i PJM_J), \tag{9}$$

where N_c is the number of CSFs, γ_i represents the additional quantum numbers needed to define the configuration, and c_i are the mixing coefficient. The radial orbitals are optimized using the extended optimal level (EOL) scheme with equal weights. The coefficients c_i are determined variationally by minimizing the energy expectation value of the Dirac–Coulomb Hamiltonian, expressed (in atomic unit) as follows:

$$\hat{H}^{DC} = c\boldsymbol{\alpha} \cdot \mathbf{p} + (\beta - 1)c^2 + \sum_{i>j}^{N} \frac{1}{r_{ij}}, \tag{10}$$

where $\boldsymbol{\alpha}$ and $\boldsymbol{\beta}$ are 4×4 Dirac matrices, p_i is the momentum operator, V_i^N is the interaction between the ith electron and the atomic nucleus, $\frac{1}{r_{ij}}$ is the electron–electron Coulomb repulsion, and c is the speed of light in vacuum.

After orbital optimization, the RCI step includes the frequency-independent Breit interaction and leading quantum electrodynamics (QED) effects—self-energy (SE) and vacuum polarization (VP)—as first-order perturbations corrections. Higher-order retardation terms beyond the ω^2 expansion are omitted. The Breit interaction in the low-frequency limit is given by the following:

$$\hat{H}_{\text{Breit}} = -\sum_{i<j}^{N} \frac{1}{2r_{ij}} \left[(\boldsymbol{\alpha}_i \cdot \boldsymbol{\alpha}_j) + \frac{(\boldsymbol{\alpha}_i \cdot \mathbf{r}_{ij})(\boldsymbol{\alpha}_j \cdot \mathbf{r}_{ij})}{r_{ij}^2} \right]. \tag{11}$$

The transition probability A_{ij} between two states is evaluated through reduced matrix elements of the multipolar radiation field operator O^L.

$$A_{ij} = \langle \Psi(\gamma PJ) \| \hat{O}^L \| \Psi(\gamma' P' J') \rangle = \sum_{i,j} c_i c_j' \langle \Psi(\gamma_i PJ) \| \hat{O}^L \| \Psi(\gamma_j' P' J') \rangle, \tag{12}$$

where c_i and c_j' are the expansion coefficients for the initial and final CSFs. The lifetime τ_i of an excited state i is then

$$\tau_i = \frac{1}{\sum_j A_{ij}}. \tag{13}$$

3.2. Electron Correlation Model

To accurately account for electron correlation effects, we construct a series of active space (AS) models using configuration state functions generated via single and double (SD) excitations from the valence orbitals into a set of virtual orbitals. Given that Sn-like ions

possess only four valence electrons, and to maintain computational tractability, we treat the closed-shell configuration $\{1s^2 2s^2 2p^6 3s^2 3p^6 3d^{10} 4s^2 4p^6 4d^{10}\}$ as inactive core. Excitation from the inactive core are not included.

In the final calculations, SD excitations are applied to the four valence electrons in the $\{5s^2 5p^2\}$ orbitals. The construction of active spaces proceeds as follows:

$$\begin{aligned} DF &= \{5s, 5p\} \\ AS1 &= DF + \{4f, 5f, 5g\} \\ AS2 &= AS1 + \{6s, 6p, 6d, 6f, 6g\} \\ AS3 &= AS2 + \{7s, 7p, 7d, 7f, 7g\} \\ AS4 &= AS3 + \{8s, 8p, 8d, 8f, 8g\} \\ AS5 &= AS4 + \{9s, 9p, 9d, 9f, 9g\} \\ AS6 &= AS5 + \{10s, 10p, 10d, 10f, 10g\}. \end{aligned}$$

To ensure convergence, virtual orbitals were expanded incrementally up to $n_{\max} = 10$ and $l_{\max} = 4$, representing the maximum principal and the angular momentum quantum number, respectively. At each step, only the newly added orbitals were optimized while previously generated orbitals were held fixed. In the GRASP2K package, the orbital orthogonality is strictly preserved throughout the self-consistent field (SCF) optimization process. The orbital sets are constructed and updated in a manner that explicitly enforces the orthogonal normality conditions, thus ensuring that the active orbitals remain always orthogonal to the frozen ones.

The excitation energies of Pr^{9+} calculated under different AS models are presented in Table 5. The result show consistent convergence with increasing active space, validating the reliability of the chosen electron correlation model.

Table 5. Convergence of MCDHF calculated excitation energies (in cm^{-1}) for selected states of Pr^{9+} across different active sets. DF represents the Dirac–Fock calculation.

	Energy (cm^{-1})					
	$5p^2$		$5p4f$			
AS	$^3P_1$	$^3P_2$	$^3G_3$	$^3F_2$	$^3F_3$	$^3G_4$
DF	27,672.04	36,470.81	21,048.52	23,645.63	25,955.64	28,098.59
AS1	28,346.58	36,989.53	21,895.37	24,144.97	26,437.06	28,669.28
AS2	28,342.42	36,950.90	21,943.95	24,181.02	26,482.04	28,704.41
AS3	28,354.15	36,985.37	22,117.35	24,318.77	26,646.55	28,872.52
AS4	28,359.17	36,980.70	22,145.11	24,340.75	26,673.04	28,894.80
AS5	28,380.26	36,995.13	22,184.96	24,374.09	26,710.83	28,931.23
AS6	28,385.66	36,996.78	22,195.03	24,381.87	26,719.68	28,939.60

4. Conclusions

In this work, we have performed a comprehensive theoretical investigation of the highly charged ions Pr^{9+} and Nd^{10+} using the multi-configuration Dirac–Hartree–Fock (MCDHF) method, including Breit interaction and QED corrections. Our calculations cover energy levels, transition probabilities, Landé g_J factors, and hyperfine interaction constants, achieving excellent agreement with available experimental data and thereby validating the reliability of our computational approach.

Through detailed angular momentum coupling analysis, we resolved ambiguities in configuration assignments and identified dominant Breit interaction effects in shaping the

fine-structure and hyperfine structures. Notably, we present the theoretical predictions of electric quadrupole hyperfine constants (B_{hfs}) for these ions.

Furthermore, we carried out an in-depth analysis of the sensitivity of clock transitions to potential variations of the fine-structure constant α. Our results reveal exceptionally large enhancement factors (K), especially in Nd^{10+}, due to strong relativistic $5p$–$4f$ orbital hybridization. This extreme sensitivity positions these ions as promising candidates for next-generation optical clocks and precision tests of fundamental physics, including searches for temporal variation in α and violations of local Lorentz invariance.

Altogether, our findings provide critical atomic data, resolve existing theoretical uncertainties, and offer valuable guidance for experimental efforts aimed at developing high-precision clocks based on alternative highly charged ions.

Author Contributions: S.Z. was involved in software, investigation, formal analysis, data curation, visualization, writing—original draft. C.W. contributed to validation. C.D. was involved in writing—review & editing. X.D. helped in conceptualization, funding acquisition, resources, supervision, writing—review & editing. All authors have read and agreed to the published version of the manuscript.

Funding: This research was funded by the National Natural Science Foundation of China (Grant No. 12274352), and the National Key Research and Development Program of China (Grant No. 2022YFA1602500).

Data Availability Statement: The datasets generated during or analysed during the current study are available from the corresponding author on reasonable request.

Conflicts of Interest: Authors Cunqiang Wu, Chenzhong Dong and Xiaobin Ding were employed by the company Gansu International Scientific and Technological Cooperation Base of Laser Plasma Spectroscopy. The remaining authors declare that the research was conducted in the absence of any commercial or financial relationships that could be construed as a potential conflict of interest.

References

1. Bekker, H.; Hensel, C.; Daniel, A.; Windberger, A.; Pfeifer, T.; Crespo López-Urrutia, J.R. Laboratory precision measurements of optical emissions from coronal iron. *Phys. Rev. A* **2018**, *98*, 062514. [CrossRef]
2. Klaft, I.; Borneis, S.; Engel, T.; Fricke, B.; Grieser, R.; Huber, G.; Kühl, T.; Marx, D.; Neumann, R.; Schröder, S.; et al. Precision Laser Spectroscopy of the Ground State Hyperfine Splitting of Hydrogenlike $^{209}Bi^{82+}$. *Phys. Rev. Lett.* **1994**, *73*, 2425–2427. [CrossRef] [PubMed]
3. Seelig, P.; Borneis, S.; Dax, A.; Engel, T.; Faber, S.; Gerlach, M.; Holbrow, C.; Huber, G.; Kühl, T.; Marx, D.; et al. Ground State Hyperfine Splitting of Hydrogenlike $^{207}Pb^{81+}$ by Laser Excitation of a Bunched Ion Beam in the GSI Experimental Storage Ring. *Phys. Rev. Lett.* **1998**, *81*, 4824–4827. [CrossRef]
4. Ullmann, J.; Andelkovic, Z.; Brandau, C.; Dax, A.; Geithner, W.; Geppert, C.; Gorges, C.; Hammen, M.; Hannen, V.; Kaufmann, S.; et al. High precision hyperfine measurements in Bismuth challenge bound-state strong-field QED. *Nat. Commun.* **2017**, *8*, 15484. [CrossRef] [PubMed]
5. Derevianko, A.; Dzuba, V.A.; Flambaum, V.V. Highly Charged Ions as a Basis of Optical Atomic Clockwork of Exceptional Accuracy. *Phys. Rev. Lett.* **2012**, *109*, 180801. [CrossRef]
6. Liang, S.Y.; Zhang, T.X.; Guan, H.; Lu, Q.F.; Xiao, J.; Chen, S.L.; Huang, Y.; Zhang, Y.H.; Li, C.B.; Zou, Y.M.; et al. Probing multiple electric-dipole-forbidden optical transitions in highly charged nickel ions. *Phys. Rev. A* **2021**, *103*, 022804. [CrossRef]
7. Berengut, J.C.; Dzuba, V.A.; Flambaum, V.V. Enhanced Laboratory Sensitivity to Variation of the Fine-Structure Constant using Highly Charged Ions. *Phys. Rev. Lett.* **2010**, *105*, 120801. [CrossRef]
8. Schiller, S. Hydrogenlike Highly Charged Ions for Tests of the Time Independence of Fundamental Constants. *Phys. Rev. Lett.* **2007**, *98*, 180801. [CrossRef]
9. Zheng, X.; Dolde, J.; Ming Lim, H.; Ranabhat, N.; Kolkowitz, S. Differential clock comparisons with a multiplexed optical lattice clock. *Nature* **2022**, *602* , 425–430 [CrossRef]
10. Nandy, D.K.; Sahoo, B.K. Highly charged W^{13+}, Ir^{16+}, and Pt^{17+} ions as promising optical clock candidates for probing variations of the fine-structure constant. *Phys. Rev. A* **2016**, *94*, 032504. [CrossRef]

11. Berengut, J.C.; Dzuba, V.A.; Flambaum, V.V.; Ong, A. Optical Transitions in Highly Charged Californium Ions with High Sensitivity to Variation of the Fine-Structure Constant. *Phys. Rev. Lett.* **2012**, *109*, 070802. [CrossRef]
12. Dzuba, V.A.; Flambaum, V.V. Highly charged ions for atomic clocks and search for variation of the fine structure constant. *Hyperfine Interact.* **2015**, *236*, 79–86. [CrossRef]
13. Bothwell, T.; Kennedy, C.J.; Aeppli, A.; Kedar, D.; Robinson, J.M.; Oelker, E.; Staron, A.; Ye, J. Resolving the gravitational redshift across a millimetre-scale atomic sample. *Nature* **2022**, *602*, 420–424. [CrossRef]
14. Arvanitaki, A.; Huang, J.; Van Tilburg, K. Searching for dilaton dark matter with atomic clocks. *Phys. Rev. D* **2015**, *91*, 015015. [CrossRef]
15. Yudin, V.I.; Taichenachev, A.V.; Derevianko, A. Magnetic-Dipole Transitions in Highly Charged Ions as a Basis of Ultraprecise Optical Clocks. *Phys. Rev. Lett.* **2014**, *113*, 233003. [CrossRef] [PubMed]
16. Dailey, C.; Bradley, C.; Jackson Kimball, D.F.; Sulai, I.A.; Pustelny, S.; Wickenbrock, A.; Derevianko, A. Quantum sensor networks as exotic field telescopes for multi-messenger astronomy. *Nat. Astron.* **2020**, *5*, 150–158. [CrossRef]
17. Ludlow, A.D.; Boyd, M.M.; Ye, J.; Peik, E.; Schmidt, P.O. Optical atomic clocks. *Rev. Mod. Phys.* **2015**, *87*, 637–701. [CrossRef]
18. Morel, L.; Yao, Z.; Cladé, P.; Guellati-Khélifa, S. Determination of the fine-structure constant with an accuracy of 81 parts per trillion. *Nature* **2020**, *588*, 61–65. [CrossRef] [PubMed]
19. Godun, R.M.; Nisbet-Jones, P.B.R.; Jones, J.M.; King, S.A.; Johnson, L.A.M.; Margolis, H.S.; Szymaniec, K.; Lea, S.N.; Bongs, K.; Gill, P. Frequency Ratio of Two Optical Clock Transitions in $^{171}Yb^{+}$ and Constraints on the Time Variation of Fundamental Constants. *Phys. Rev. Lett.* **2014**, *113*, 210801. [CrossRef]
20. Sang, C.C.; Chen, Z.B.; Sun, Y.; Shen, X.Z.; Hu, F.; Ma, J.; Wang, X.L. Hyperfine structure and 2s-2p transition in C-like Fe, Co and Ni. *J. Electron Spectrosc. Relat. Phenom.* **2019**, *230*, 26–32. [CrossRef]
21. Grunefeld, S.J.; Roberts, B.M.; Ginges, J.S.M. Correlation trends in the hyperfine structure for Rb, Cs, and Fr, and high-accuracy predictions for hyperfine constants. *Phys. Rev. A* **2019**, *100*, 042506. [CrossRef]
22. Safronova, M.S.; Budker, D.; DeMille, D.; Kimball, D.F.J.; Derevianko, A.; Clark, C.W. Search for new physics with atoms and molecules. *Rev. Mod. Phys.* **2018**, *90*, 025008. [CrossRef]
23. Koike, F.; Suzuki, C.; Murakami, I.; Kato, D.; Tamura, N.; Nakamura, N. Z -dependent crossing of excited-state energy levels in highly charged galliumlike lanthanide atomic ions. *Phys. Rev. A* **2022**, *105*, 032802. [CrossRef]
24. Rosenband, T.; Hume, D.B.; Schmidt, P.O.; Chou, C.W.; Brusch, A.; Lorini, L.; Oskay, W.H.; Drullinger, R.E.; Fortier, T.M.; Stalnaker, J.E.; et al. Frequency Ratio of Al^{+} and Hg^{+} Single-Ion Optical Clocks; Metrology at the 17th Decimal Place. *Science* **2008**, *319*, 1808–1812. [CrossRef]
25. Brewer, S.M.; Chen, J.S.; Hankin, A.M.; Clements, E.R.; Chou, C.w.; Wineland, D.J.; Hume, D.B.; Leibrandt, D.R. $^{27}Al^{+}$ quantum-logic clock with a systematic uncertainty below 10^{-18}. *Phys. Rev. Lett.* **2019**, *123*, 033201. [CrossRef]
26. Chou, C.; Hume, D.; Koelemeij, J.; Wineland, D.; Rosenband, T. Frequency Comparison of Two High-Accuracy Al^{+} Optical Clocks. *Phys. Rev. Lett.* **2010**, *104*, 070802. [CrossRef]
27. Chou, C.W.; Hume, D.B.; Rosenband, T.; Wineland, D.J. Optical Clocks and Relativity. *Science* **2010**, *329*, 1630–1633. [CrossRef] [PubMed]
28. Yu, Y.M.; Sahoo, B.K.; Suo, B.B. Highly charged ion (HCI) clocks: Frontier candidates for testing variation of fine-structure constant. *Front. Phys.* **2023**, *11*, 1104848. [CrossRef]
29. Yu, Y.m.; Sahoo, B.K. Energy-level-crossing study of forbidden transitions in highly charged ions with $(n=4,5)d^6$ and $(n=4,5)d^8$ configurations for making optical clocks. *Phys. Rev. A* **2024**, *109*, 023106. [CrossRef]
30. Levine, J.S.; Bonczyk, P.A.; Javan, A. Observation of Hyperfine Level Crossing in Stimulated Emission. *Phys. Rev. Lett.* **1969**, *22*, 267–270. [CrossRef]
31. Beloy, K.; Dzuba, V.A.; Brewer, S.M. Quadruply Ionized Barium as a Candidate for a High-Accuracy Optical Clock. *Phys. Rev. Lett.* **2020**, *125*, 173002. [CrossRef] [PubMed]
32. Bekker, H.; Borschevsky, A.; Harman, Z.; Keitel, C.H.; Pfeifer, T.; Schmidt, P.O.; Crespo López-Urrutia, J.R.; Berengut, J.C. Detection of the 5p – 4f orbital crossing and its optical clock transition in Pr^{9+}. *Nat. Commun.* **2019**, *10*, 5651 [CrossRef] [PubMed]
33. Porsev, S.G.; Safronova, U.I.; Safronova, M.S.; Schmidt, P.O.; Bondarev, A.I.; Kozlov, M.G.; Tupitsyn, I.I.; Cheung, C. Optical clocks based on the Cf^{15+} and Cf^{17+} ions. *Phys. Rev. A* **2020**, *102*, 012802. [CrossRef]
34. Yu, Y.; Pan, D.; Chen, S.; Arora, B.; Guan, H.; Gao, K.; Chen, J. Atomic Structure of Nd^{9+} for Highly Charged Ion Clocks. *Atoms* **2022**, *10*, 123. [CrossRef]
35. Safronova, M.S.; Dzuba, V.A.; Flambaum, V.V.; Safronova, U.I.; Porsev, S.G.; Kozlov, M.G. Highly Charged Ions for Atomic Clocks, Quantum Information, and Search for α variation. *Phys. Rev. Lett.* **2014**, *113*, 030801. [CrossRef]
36. Dzuba, V.A.; Safronova, M.S.; Safronova, U.I.; Flambaum, V.V. Actinide ions for testing the spatial α-variation hypothesis. *Phys. Rev. A* **2015**, *92*, 060502. [CrossRef]
37. Berengut, J.C.; Dzuba, V.A.; Flambaum, V.V.; Ong, A. Electron-Hole Transitions in Multiply Charged Ions for Precision Laser Spectroscopy and Searching for Variations in α. *Phys. Rev. Lett.* **2011**, *106*, 210802. [CrossRef]

38. Porsev, S.G.; Ludlow, A.D.; Boyd, M.M.; Ye, J. Determination of Sr properties for a high-accuracy optical clock. *Phys. Rev. A* **2008**, *78*, 032508. [CrossRef]
39. Wang, G.; Lu, Z.; Liang, X.; He, K.; He, Y.; Ji, X. Optical Frequency Transfer on the Order of 10^{-19} Fractional Frequency Instability over a 64 m Free-Space Link. *Photonics* **2024**, *11*, 587. [CrossRef]
40. King, S.A.; Spieß, L.J.; Micke, P.; Wilzewski, A.; Leopold, T.; Benkler, E.; Lange, R.; Huntemann, N.; Surzhykov, A.; Yerokhin, V.A.; et al. An optical atomic clock based on a highly charged ion. *Nature* **2022**, *611*, 43–47. [CrossRef]
41. Lyu, C.; Keitel, C.H.; Harman, Z. Ultrastable and ultra-accurate clock transitions in open-shell highly charged ions. *Commun. Phys.* **2025**, *8*, 3. [CrossRef]
42. Liu, X.; Zhou, X.P.; Wen, W.Q.; Lu, Q.F.; Yan, C.L.; Xu, G.Q.; Xiao, J.; Huang, Z.K.; Wang, H.B.; Chen, D.Y.; et al. Spectral calibration for electron beam ion trap and precision measurement of M1 transition wavelength in Ar^{13+}. *Acta Phys. Sin.* **2022**, *71*, 033201. [CrossRef]
43. Safronova, M.S.; Dzuba, V.A.; Flambaum, V.V.; Safronova, U.I.; Porsev, S.G.; Kozlov, M.G. Atomic properties of Cd-like and Sn-like ions for the development of frequency standards and search for the variation of the fine-structure constant. *Phys. Rev. A* **2014**, *90*, 052509. [CrossRef]
44. Berengut, J.C.; Dzuba, V.A.; Flambaum, V.V.; Ong, A. Highly charged ions with E1,M1, and E2 transitions within laser range. *Phys. Rev. A* **2012**, *86*, 022517. [CrossRef]
45. Kozlov, M.G.; Safronova, M.S.; Crespo López-Urrutia, J.R.; Schmidt, P.O. Highly charged ions: Optical clocks and applications in fundamental physics. *Rev. Mod. Phys.* **2018**, *90*, 045005. [CrossRef]
46. Chen, S.; Zhou, Z.; Li, J.; Zhang, T.; Li, C.; Shi, T.; Huang, Y.; Gao, K.; Guan, H. Precision measurement of M1 optical clock transition in Ni^{12+}. *Phys. Rev. Res.* **2024**, *6*, 013030. [CrossRef]
47. Murata, S.; Nakajima, T.; Safronova, M.S.; Safronova, U.I.; Nakamura, N. Visible transitions in Ag-like and Cd-like lanthanide ions. *Phys. Rev. A* **2017**, *96*, 062506. [CrossRef]
48. Fischer, C.F.; Verdebout, S.; Godefroid, M.; Rynkun, P.; Jönsson, P.; Gaigalas, G. Toward Calculations with Spectroscopic Accuracy: The $2s^2 2p\ ^2P_{3/2}$ - $2s2p^2\ ^4P_{5/2}$ Excitation Energy in Boron. *arXiv* **2013**, arXiv:1310.2394. . [CrossRef]
49. Porsev, S.G.; Cheung, C.; Safronova, M.S.; Bekker, H.; Rehbehn, N.H.; López-Urrutia, J.R.C.; Brewer, S.M. Pr^{10+} as a candidate for a high-accuracy optical clock for tests of fundamental physics. *Phys. Rev. A* **2024**, *110*, 042823. [CrossRef]
50. Stone, N. Table of nuclear magnetic dipole and electric quadrupole moments. *At. Data Nucl. Data Tables* **2005**, *90*, 75–176. [CrossRef]
51. Lu, B.; Chang, H. Theoretical calculations on Landé g-factors and quadratic Zeeman shift coefficients of nsnp $^3P_0$ clock states in Mg and Cd optical lattice clocks. *Chin. Phys. B* **2023**, *32*, 013101. [CrossRef]
52. Wu, C.; Dong, C.; Ding, X. Precision investigations of clock transitions and metastable lifetimes in highly charged Te-like ions. *Phys. Lett. A* **2024**, *522*, 129805. [CrossRef]
53. Salhi, D.E.; Nasr, S.B.; Manai, S.; Jelassi, H. Multiconfiguration Dirac–Hartree–Fock energy levels, weighted oscillator strengths, transitions probabilities, lifetimes, hyperfine interaction constants, Landé g-factors and isotope shifts of O VII. *Results Phys.* **2021**, *23*, 103960. [CrossRef]
54. Liu, M.; Li, B.B.; Wu, L.; Jiang, J. The Landé g factors of highly charged Sn^{47+} and Bi^{80+} ions. *Phys. Scr.* **2024**, *99*, 055406. [CrossRef]
55. Marques, J.P.; Indelicato, P.; Parente, F.; Sampaio, J.M.; Santos, J.P. Ground-state Landé g factors for selected ions along the boron isoelectronic sequence. *Phys. Rev. A* **2016**, *94*, 042504. [CrossRef]
56. Huntemann, N.; Sanner, C.; Lipphardt, B.; Tamm, C.; Peik, E. Single-Ion Atomic Clock with 3×10^{-18} Systematic Uncertainty. *Phys. Rev. Lett.* **2016**, *116*, 063001. [CrossRef] [PubMed]
57. Gilles, J.; Fritzsche, S.; Spieß, L.J.; Schmidt, P.O.; Surzhykov, A. Quadratic Zeeman and Electric Quadrupole Shifts in Highly Charged Ions. *arXiv* **2024**, arXiv:2411.05687.
58. Cheng, K.T.; Childs, W.J. Ab initio calculation of $4f^N 6s^2$ hyperfine structure in neutral rare-earth atoms. *Phys. Rev. A* **1985**, *31*, 2775–2784. [CrossRef]
59. Flambaum, V.V.; Dzuba, V.A. Search for variation of the fundamental constants in atomic, molecular, and nuclear spectra. *Can. J. Phys.* **2009**, *87*, 25–33. [CrossRef]
60. Allehabi, S.O.; Dzuba, V.A.; Flambaum, V.V. Atomic clocks highly sensitive to the variation of the fine-structure constant based on Hf II, Hf IV, and W VI ions. *Phys. Rev. A* **2022**, *106*, 032807,
61. Allehabi, S.O.; Brewer, S.M.; Dzuba, V.A.; Flambaum, V.V.; Beloy, K. High-accuracy optical clocks based on group-16-like highly charged ions. *Phys. Rev. A* **2022**, *106*, 043101. [CrossRef]
62. Jonsson, P.; He, X.; Froese Fischer, C.; Grant, I. The Grasp2K relativistic atomic structure package. *Comput. Phys. Commun.* **2007**, *177*, 597–622. [CrossRef]
63. Jonsson, P.; Gaigalas, G.; Bieroń, J.; Fischer, C.F.; Grant, I. New version: Grasp2K relativistic atomic structure package. *Comput. Phys. Commun.* **2013**, *184*, 2197–2203. [CrossRef]

64. Jonsson, P.; Gaigalas, G.; Fischer, C.F.; Bieroń, J.; Grant, I.P.; Brage, T.; Ekman, J.; Godefroid, M.; Grumer, J.; Li, J.; et al. GRASP Manual for Users. *Atoms* **2023**, *11*, 68. [CrossRef]
65. Fischer, C.F.; Godefroid, M.; Brage, T.; Jönsson, P.; Gaigalas, G. Advanced multiconfiguration methods for complex atoms: I. Energies and wave functions. *J. Phys. B At. Mol. Opt. Phys.* **2016**, *49*, 182004. [CrossRef]
66. Grant, I.P. *Relativistic Quantum Theory of Atoms and Molecules: Theory and Computation*; Springer: New York, NY, USA, 2007.
67. Wu, C.; Ding, X.; Cao, M.; Zhang, D.; Zhang, M.; Xue, Y.; Yu, D.; Dong, C. Energy levels and radiative transition properties of the 2s2p double K-shell vacancy state in He-like ions. *At. Data Nucl. Data Tables* **2023**, *154*, 101602. [CrossRef]
68. Wu, C.; Zhao, R.; Zhang, D.; Zhang, M.; Xue, Y.; Yu, D.; Dong, C.; Ding, X. The influence of relativistic, Breit interaction, and QED effects on the $1s^2 2p^2$ and $2s2p^3$ energy levels of Be-like ($4 \leq Z \leq 74$) isoelectronic sequence. *Eur. Phys. J. D* **2023**, *77*, 129. [CrossRef]